TRENDS IN SCIENCES 2026; 23(8): 13057
https://doi.org/10.48048/tis.2026.13057 RESEARCH ARTICLE

Herbal Multi-Target Strategy Against Ovarian Cancer: *In Silico* Evaluation of *Elephantopus scaber* Phytoconstituents Targeting PI3K, BCL-2, and VEGFR-2

Yuyun Ika Christina[1,2], Shella Zahra Kumala Azmi[3], Wirdatun Nafisah[4], Honesty Nurizza Pinanti[4], Muhammad Hermawan Widyananda[5], Sutrisno Sutrisno[6], Elok Zubaidah[2,7], Husnul Khotimah[2,8] and Muhammad Sasmito Djati[1,2,3,*]

[1]*Innovation Center of Integrative Jamu and Eco-pharmaca, Brawijaya University, East Java 65145, Indonesia*
[2]*Dewan Jamu Indonesia East Java Region, East Java 65145, Indonesia*
[3]*Department of Biology, Faculty of Mathematics and Natural Sciences, Brawijaya University, East Java 65145, Indonesia*
[4]*Department of Biology, Faculty of Mathematics and Science, Universitas Negeri Surabaya, East Java 60231, Indonesia*
[5]*Biosystem Study Center, Brawijaya University, East Java 65145, Indonesia*
[6]*Division of Reproductive Endocrinology and Infertility, Department of Obstetrics and Gynaecology, Faculty of Medicine, University of Brawijaya, Saiful Anwar General Hospital, East Java 65145, Indonesia*
[7]*Department of Food Science and Technology, Faculty of Agricultural Technology, Brawijaya University, East Java 65145, Indonesia*
[8]*Laboratory of Pharmacology, Faculty of Medicine, Brawijaya University, East Java 65145, Indonesia*

([*]Corresponding author's e-mail: msdjati@ub.ac.id)

Received: 16 December 2025, Revised: 3 February 2026, Accepted: 10 February 2026, Published: 20 March 2026

Abstract

Ovarian cancer continues to be one of the deadliest gynecologic cancers, mainly due to delayed diagnosis and treatment resistance. For the treatment of ovarian cancer, a multi-target therapeutic approach that targets key signaling pathways, including PI3K-mediated cell survival, BCL-2-regulated apoptosis, and VEGFR-2-driven angiogenesis, is considered promising. Therefore, using an *in silico* approach targeting VEGFR-2, BCL-2, and PI3K, this work sought to explore the anticancer potential of phytochemical compounds from the *Elephantopus scaber* L. extract. After identifying bioactive chemicals from E. scaber by LC-HRMS analysis, AutoDock Vina was used to perform molecular docking against VEGFR-2, BCL-2, and PI3K. SwissADME was used to predict drug-likeness and pharmacokinetic properties, and pkCSM was used to investigate toxicity profiles. Several compounds from the *E. scaber* extract exhibited substantial binding affinities for the selected targets, as determined by molecular docking. Genistin (−10.1 kcal/mol), apigenin-7-O-glucuronide (−9.9 kcal/mol), and luteolin (−9.6 kcal/mol) demonstrated stronger interactions with VEGFR-2 than the reference inhibitor nintedanib (−7.0 kcal/mol). Additionally, apigenin-7-O-glucuronide had a greater affinity for binding BCL-2 (−7.5 kcal/mol) than obatoclax (−6.8 kcal/mol). While slightly weaker than alpelisib (−10.5 kcal/mol), apigenin-7-O-glucuronide (−9.7 kcal/mol), genistin (−9.3 kcal/mol), and scutellarin (−9.2 kcal/mol) showed the most advantageous contacts in PI3K docking. Most selected compounds fulfilled drug-likeness criteria and displayed low predicted toxicity. The findings highlight *E. scaber* as a promising source of multi-target anticancer phytochemicals, with apigenin-7-O-glucuronide and genistin emerging as the most potent candidates for further experimental validation.

Keywords: *Elephantopus scaber*, BCL2, Ovarian cancer, Molecular docking, PI3K, VEGFR-2, *In silico*, Phytochemicals

Introduction

Ovarian cancer is one of the most lethal gynecologic malignancies globally, primarily due to the asymptomatic nature of its early stages and the limited efficacy of current treatments in advanced disease stages [1,2]. In 2022, approximately 324,603 new cases of ovarian cancer were found in women worldwide. The World Ovarian Cancer Coalition [3] estimated that the annual incidence in 2050 will have risen by 55%. A high increase in new cases was found in Asia by 178,223 (2022) and then estimated to increase by 2050 to 265,900 [4,5]. The World Cancer Research Fund reported that Indonesia had the fourth-highest number of cases and deaths from ovarian cancer in 2022. World Cancer Research Fund reported 15,130 new cases in 2022, with 9,673 deaths. Despite advances in surgical techniques and chemotherapeutic regimens, the overall five-year survival rate for ovarian cancer patients remains below 45%, especially in cases diagnosed at later stages [6]. This underscores the urgent need for new drugs to effectively target key oncogenic pathways implicated in tumor resistance and progression.

Complex molecular networks encompassing several oncogenic pathways are responsible for the progression of ovarian cancer and treatment resistance [7]. The phosphoinositide 3-kinase (PI3K) pathway, which regulates cell survival, proliferation, apoptosis, and metabolism, is a crucial signaling axis [8,9]. Chemoresistance and a poor prognosis are linked to dysregulation of this system, which is commonly seen in ovarian malignancies [10]. Furthermore, a crucial anti-apoptotic protein, B-cell lymphoma 2 (BCL-2), promotes resistance to cytotoxic therapies by preventing mitochondrial apoptosis, thereby helping tumor cells survive [11]. Additionally, by encouraging vascularization and nutrition supply, angiogenesis mediated by vascular endothelial growth factor receptor 2 (VEGFR-2) is crucial for tumor development, invasion, and metastasis [12]. The argument for a multi-target treatment approach is supported by the fact that PI3K, BCL2, and VEGFR-2 are highly relevant therapeutic targets due to their prominent roles in ovarian cancer.

Natural products derived from medicinal plants offer a rich repository of structurally diverse bioactive compounds with significant anticancer potential. Among these, *Elephantopus scaber* L., commonly known as Tapak Liman, is a traditional medicinal herb widely used in Southeast Asian ethnomedicine to treat fever, infections, inflammation, and liver disorders [13, 14]. According to phytochemical studies, *E. scaber* contains several bioactive metabolites, including flavonoids, triterpenoids, and sesquiterpene lactones (deoxyelephantopin), which have demonstrated cytotoxic and antiproliferative actions in various cancer cell lines [15-16].

The molecular underpinnings of *E. scaber*'s anticancer activity, particularly in ovarian cancer, remain poorly understood. Furthermore, insufficient research has been conducted on its ability to concurrently modulate multiple cancer-related targets. In this study, we employed a computational approach to explore the potential of selected phytoconstituents from *E. scaber* to interact with and inhibit key proteins within the PI3K/AKT/mTOR signaling cascade and VEGFR-2. Using molecular docking, drug-likeness analysis, and toxicity prediction, this research aims to provide mechanistic insights and identify lead compounds for further in vitro and in vivo investigation as multi-target herbal-based anticancer agents.

Materials and methods

Plant extraction

Plant extraction was performed using the maceration method previously described by Christina *et al.* [17] and Alghoull *et al.* [18]. *E. scaber* powder was purchased from the UPT. Laboratorium Herbal Materia Medica, Batu (7°52'01.2"S and 112°31'13.2"E), with identification number 067/656/102.20/2023. *E. scaber* powder (100 g) was diluted with 1,000 mL of 95% ethanol. The mixture was incubated at room temperature for 24 h. The mixture was filtered and then evaporated using a rotary evaporator at 70 °C. The crude extract was stored at 4 °C.

Identification and selection of bioactive compounds in *E. scaber* crude extract

The analysis method using Liquid Chromatography–High Resolution Mass Spectrometry (LC-HRMS) followed the protocol of Christina *et al.* [18]. The *E. scaber* constituent was separated using Dionex Ultimate 3000 RSLCnano with a microflow meter (Thermo Fisher Scientific Inc., USA). A Hypersil GOLD aQ C18 Polar Endcapped HPLC Column

(Thermo Fisher Scientific Inc., USA) with dimensions of 50×1mm×1.9 µm particle size was used. Solvent A was 0.1% formic acid in water, and solvent B was 0.1% formic acid in acetonitrile. Positive ion mode detection was performed using Q Exactive Orbitrap Mass Spectrometers (Thermo Fisher Scientific Inc., USA). The compounds were identified using Compound Discoverer software and the mzCloud MS/MS library (https://www.mzcloud.org/). The bioactive compounds of the ethanol extract of *E. scaber* leaves were then identified based on LC-HRMS profiling data. Twenty-five compounds were selected based on mzCloud Best Match values (>80) derived from LC-HRMS data [19].

Screening of drug likeness and anticancer activity prediction

The canonical SMILES of *E. scaber* compounds were obtained from the PubChem database (https://pubchem.ncbi.nlm.nih.gov/). The compounds were screened for drug likeness using the SWISSADME web server (https://www.swissadme.ch/) [20]. Drug likeness screening was used to identify compounds with potential medicinal properties following the Lipinski, Ghose, Veber, Egan, and Muegge rules [21]. The PASS Online web server (https://www.way2drug.com/passonline/) was used to screen for possible biological activities related to anticancer [21], including BRAF expression inhibitor, TNF expression inhibitor, TP53 expression enhancer, apoptosis agonist, HIF1A expression inhibitor, JAK2 expression inhibitor, kinase inhibitor, MMP9 expression inhibitor, caspase 3 stimulant, and caspase 8 stimulant. To achieve the highest prediction of the active compound's activity, a cut-off value for probable activity (Pa) greater than 0.7 was used.

Prediction of pharmacokinetics and toxicity

The pharmacokinetic and toxicity properties of selected phytochemicals from *E. scaber* extract were predicted using the pkCSM web server (https://biosig.lab.uq.edu.au/pkcsm/) [22]. The predicted ADMET (absorption, distribution, metabolism, excretion, and toxicity) parameters such as water solubility, Caco-2 permeability, human intestinal absorption, P-glycoprotein substrate/inhibitor status, volume of distribution (VDss), and blood–brain barrier permeability.

Molecular docking analysis

The selected bioactive compound of *E. scaber* was subjected to molecular docking with its designated target protein. First, three-dimensional crystal structures of target proteins, including PI3K (4JPS), BCL-2 (1G5M), and VEGFR-2 (2OH4), were obtained from the PDB RCSB database (https://www.rcsb.org/). Before docking, all protein structures were prepared by removing co-crystallized ligands, water molecules, and ions using Open Babel. Ligand structures were energy-minimized using the MMFF94 force field to obtain stable conformations using Open Babel in the PyRx software [23]. All ligands were subsequently converted into .pdb format. The inhibitors of each protein were nintedanib for VEGFR inhibitor (CID: 135423438), Obatoclax for BCL-2 (CID: 11404337), and Alpelisib for PI3K (CID: 56649450). The grid box parameters for specific docking were set up at the active site of each protein (**Table 1**), including VEGFR2 (X: 19.7298 Å, Y: 27.9921 Å, Z: 18.9704 Å) [24], BCL-2 (X: 29.1680 Å, Y: 25.0000 Å, Z: 21.7806 Å) [25], and PI3K (X: 23.3460 Å, Y: 24.5914 Å, Z: 24.2319Å) [26].

Molecular docking was performed using AutoDock Vina in the PyRx software to predict binding affinity and interaction modes between ligands and target proteins. The docking process was validated by re-docking the ligand and protein using the same parameters to check the consistency in the binding pose. The Root Mean Square Deviation (RMSD) value between the re-docked and crystallographic structure was calculated. The RMSD value less than 2 Å was considered acceptable for docking reliability. The docking simulation was carried out using an exhaustiveness value of 8 (**Table 1**).

Table 1 The details of the molecular docking protocol.

Protein	PDB ID	Reference inhibitor	Grid box parameters		Exhaustiveness	Redocking RMSD (Å)
			Center	Dimension (Å)		
PI3K	4JPS	Alpelisib	X: -0.2037 Y: -8.2963 Z: 16.9623	X: 23.3460 Å, Y: 24.5914 Å, Z: 24.2319Å	8	1.638
BCL-2	1G5M	Obatoclax	X: 11.8737 Y: -4.1815 Z: -7.2134	X: 29.1680 Å, Y: 25.0000 Å, Z: 21.7806 Å	8	1.376
VEGFR-2	2OH4	Nintedanib	X: 3.4578 Y: 38.0208 Z: 15.3025	X: 19.7298 Å, Y: 27.9921 Å, Z: 18.9704 Å	8	1.789

For additional examination, docking positions with the lowest binding energy were chosen. Biovia Discovery Studio 2019 (Dassault Systèmes Biovia, USA) was used to depict the optimal docking conformations to examine ligand-protein interactions, including hydrophobic contacts, hydrogen bonds, and important amino acid residues implicated in binding. The binding pose of the selected compound of *E. scaber* and the inhibitor of each protein was compared.

Molecular dynamics simulation

The molecular dynamics simulation was performed based on a previous study by Widyananda *et al.* [27]. This method was carried out using Yet Another Scientific Artificial Reality Application (YASARA) software coupled with the AMBER14 force field. The environmental settings were adjusted to mimic physiological requirements, including 37 °C, pH 7.4, 0.9% salt concentration, and 1 atm pressure, and run for 20 ns. The running simulation was carried out utilizing the md_run macro program. The simulation was executed using the md_run macro program, and the resulting data were analyzed using md_analyze to assess the root mean square deviation (RMSD) of the protein backbone and the RMSD of ligand movement.

Data analysis

Compounds having multi-target inhibitory potential were found by comparing the docking data across targets. Promising candidates for additional experimental validation included compounds with good binding affinity, pleasant interaction patterns, acceptable drug-likeness, and low projected toxicity.

Results and discussion

Identification of *E. scaber* constituent

Phytochemical profiling of *E. scaber* leaves ethanol extract effectively found 61 compounds based on their molecular formula/mass, retention time, and peak area (Supplementary **Table 1**). The mzCloud best match score (>80) and the availability of canonical SMILES and PubChem CID for standardized computer analysis were the main factors used to drive compound selection. In order to predict the biological activity associated with anticancer potential, 25 representative compounds were chosen for PASS online (**Table 2**).

Table 2 The identified compound in the *E. scaber* leaves extract based on the mzCloud best match score.

No	Name	Formula	Molecular weight	RT (min)	Area (Max.)	MzCloud Best match score
1	9-OxoODA	$C_{18}H_{30}O_3$	294.21898	12.962	204,805,241.68	93.1
2	3-Hydroxyfluorene	$C_{13}H_{10}O$	182.07292	8.52	63,513,358.69	84
3	(-)-Caryophyllene oxide	$C_{15}H_{24}O$	220.18236	13.421	43,491,453.35	91.8
4	Luteolin	$C_{15}H_{10}O_6$	286.04738	6.972	36,603,052.17	94.4

No	Name	Formula	Molecular weight	RT (min)	Area (Max.)	MzCloud Best match score
5	(+)-ar-Turmerone	$C_{15}H_{20}O$	216.15125	12.679	18,140,163.54	88.8
6	Chlorogenic acid	$C_{16}H_{18}O_9$	354.09462	2.731	12,687,054.47	90.9
7	(+/-)12(13)-DiHOME	$C_{18}H_{34}O_4$	296.23467	13.96	11,455,541.38	88.7
8	Apigenin	$C_{15}H_{10}O_5$	270.05235	7.928	10,865,967.75	91.6
9	9(Z),11(E),13(E)-Octadecatrienoic Acid methyl ester	$C_{19}H_{32}O_2$	292.23979	14.63	8,946,579.60	93.5
10	2H-cyclohepta[b]furan-2-one	$C_{15}H_{20}O_3$	230.13037	6.395	6,316,897.18	89.6
11	Scutellarin	$C_{21}H_{18}O_{12}$	462.07942	5.265	5,642,526.04	81.9
12	Oleanolic acid	$C_{30}H_{48}O_3$	438.34892	18.284	5,007,377.23	83.7
13	Apigenin 7-O-glucuronide	$C_{21}H_{18}O_{11}$	446.08431	5.755	2,941,601.43	90.6
14	Pinocembrin	$C_{15}H_{12}O_4$	256.07329	9.51	2,252,180.90	82.6
15	Schaftoside	$C_{26}H_{28}O_{14}$	564.14733	4.523	2,110,762.18	89.3
16	Shogaol	$C_{17}H_{24}O_3$	276.17238	9.405	1,908,442.62	80.9
17	(9cis)-Retinal	$C_{20}H_{28}O$	284.21349	12.787	1,776,384.42	84.1
18	Caffeic acid	$C_9H_8O_4$	180.04207	3.635	1,691,585.18	82.2
19	Sesquiterpene Lactone Cp-1	$C_{15}H_{20}O_3$	248.1409	6.395	1,063,304.72	91.5
20	4-Methylumbelliferone	$C_{10}H_8O_3$	176.04708	7.092	912,561.22	81.5
21	3-Methoxycinnamic acid	$C_{10}H_{10}O_3$	160.05225	8.515	697,221.12	83.4
22	Genistin	$C_{21}H_{20}O_{10}$	432.10515	5.702	644,072.95	80.3
23	Vitexin	$C_{21}H_{20}O_{10}$	432.10515	5.013	562,072.53	82.7
24	4-O-Feruloylquinic acid	$C_{17}H_{20}O_9$	368.11025	4.53	452,544.11	86.6
25	Verrucarol	$C_{15}H_{22}O_4$	266.15148	3.905	433,826.12	81.9

Drug likeness screening, bioactivity prediction, and pharmacokinetic absorption profile

The predicted possible interactions between several phytochemical substances discovered in *E. scaber* and molecular targets that are critical to the development of cancer are shown in **Figure 1**. Compounds' bioactivity was predicted using PASS Online using QSAR principles; a minimum Pa (Probability of activity) value of 0.3 or higher denotes the presence of specific bioactivities [28]. According to the study, the *E. scaber* leaf extract's luteolin, 9-cis retinal, 9-oxoODA, and oleanolic acid show strong activity in several pathways that support apoptosis mechanisms, such as apoptosis agonist activity, stimulation of caspase-3 and caspase-8, and increased expression of the tumor suppressor gene TP53. Moreover, 9-cis retinal, 9-oxoODA, and (+/−)12(13)-DiHOME have substantial bioactivity as BRAF expression inhibitors, which may suppress the expression of growth factors and oncogenes. Additionally, apigenin, luteolin, vitexin, and 9-oxoODA show promise as HIF1A expression inhibitors, which are implicated in cellular adaptation to hypoxic circumstances. 3-Hydroxyfluorene exhibits a strong interaction with the JAK2 expression inhibition pathway, which is linked to the control of inflammation

and cell division. Additionally, Sesquiterpene Lactone Cp-1 and 9-cis retinal have Pa values for MMP9 expression suppression, which may stop extracellular matrix degradation, a crucial step in the invasion and dissemination of cancer cells.

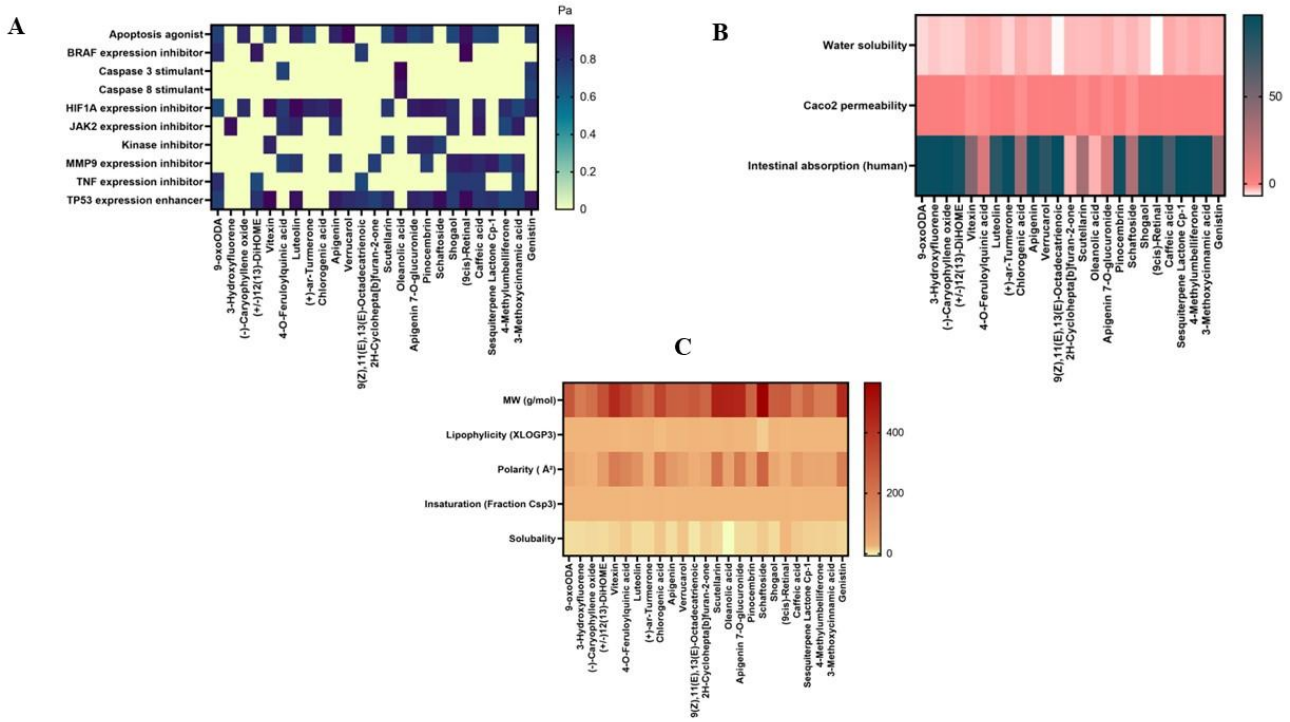

Figure 1 Drug likeness screening (A), bioactivity prediction (B), and pharmacokinetic absorption profile, and (C) of bioactive compounds of *E. scaber*

Further supporting the multipathway anticancer potential of vitexin and pinocembrin is their identification as kinase inhibitors. Through multipathway methods combining apoptosis induction, proliferation pathway inhibition, and metastasis prevention, **Figure 1** indicates that a combination of particular chemicals, specifically luteolin, 9-cis retinal, and 9-oxoODA, offers great potential as anticancer candidates. Luteolin, a naturally occurring flavone, has been shown to have strong anticancer potential in earlier research. It lowers inflammation, prevents the development, migration, and invasion of cancer cells, and encourages the death of malignant cells through autophagy and apoptosis. Furthermore, when used with traditional chemotherapy, luteolin can increase its effectiveness. By focusing on cellular processes such as apoptosis, cell cycle progression, angiogenesis, and migration, luteolin inhibits the formation of tumors. Mechanistically, it causes cell death by upregulating BAX, caspase-3, and p21 and downregulating Akt, PLK-1, cyclin-B1, cyclin-A, CDC-2, CDK-2, Bcl-2, and Bcl-xL. Additionally, by inhibiting STAT3 activation and encouraging STAT3 protein degradation in a variety of cancer cells, it suppresses STAT3 signaling [29]. In the meantime, 9-oxoODA exhibits promise as a treatment for HPV-induced cervical cancer. This substance inhibits the growth of cancer cells, slows the cell cycle, and induces partial apoptosis by suppressing the production of high-risk HPV oncoproteins such as E6 and E7 and lowering CDK1 levels. Furthermore, 9-oxoODA is a strong PPARα ligand that inhibits the development of cancer cells by regulating lipid metabolism and controlling the cell cycle through p16INK4a activation [30].

Several criteria, such as water solubility, Caco-2 cell permeability, and human intestine absorption, were used to assess the absorption of bioactive chemicals from *E. scaber*. The logS parameter, which shows solubility concentration in mol/L, was used to measure water solubility. As evidenced by the prevalence of a

pink hue and an average logS value of −3.554, most compounds generally showed low water solubility. The synthetic chemical 9oxoODA has a high permeability through Caco-2 cells, with the highest value of 1.547, according to the analysis results. Caco-2 cells are frequently used to evaluate the permeability of substances taken orally because they resemble human intestinal epithelium both morphologically and functionally. The logarithm of the apparent permeability coefficient, or log Papp, is used to express Caco-2 permeability; compounds with log Papp values higher than 0.9 are regarded as having high permeability [31]. Several substances, such as 9oxoODA, 3-Hydroxyfluorene, (−)-Caryophyllene oxide, and 9cis-retinal, demonstrated average Caco-2 permeability values of approximately 1.5, indicating their capacity to cross intestinal cell membranes. Furthermore, substances like 9cis-retinal, (+) ar-tumerone, 3-methoxycinnamic acid, and sesquiterpene Lactone Cp-1 exhibited outstanding absorption probabilities, ranging from 94% to 96%, according to computed human intestine absorption values, indicating better potential to reach optimal bioavailability. If a compound's absorption value is greater than 80%, it is deemed to have high absorption; if it is less than 30%, it is seen to have poor absorption. Orally given medications are primarily absorbed in the intestine [32]. Therefore, several possibilities, like 9cis-retinal, (+) ar-tumerone, 3-methoxycinnamic acid, and sesquiterpene Lactone Cp-1, stand out due to their promising potential for effective intestinal absorption, even if many compounds show limitations in solubility and permeability.

The physical characteristics of different *E. scaber* compounds, such as molecular weight (MW), lipophilicity (LogP), polarity, insaturation (Fraction Csp3), and solubility, are shown in **Figure 1(C)**. Pale yellow denotes low levels, and dark red denotes high values. Lipinski's Rule of Five, which states that a compound with a high likelihood of being drug-like should have a MW ≤500 daltons, hydrogen bond acceptors ≤10, hydrogen bond donors ≤5, LogP ≤5, and a molar refractivity between 40 and 130, can be used to assess each compound's potential as a drug candidate based on this data. A compound is more likely to show good bioactivity and sufficient bioavailability if it satisfies at least two of these requirements. Thus, in accordance with Lipinski's principles, this heatmap not only makes it easier to compare the chemical features of different compounds, but it also acts as a useful tool for screening those that are most similar to drug-like characteristics [33]. The only compound with a molecular weight (MW) of less than 500 daltons is shaftoside. Except for oleanolic acid and 9(Z),11(E),13(E)-Octadecatrienoic acid, the majority of compounds show lipophilicity (XLOGP3) below 5. A balance between water solubility and membrane permeability is shown by a polarity range of 20 - 130 Å^2. A balanced degree of carbon saturation is indicated by the insaturation criterion (Fraction Csp3), which lies between 0.3 and 1.0. Sufficient water solubility for absorption is indicated by solubility values between 0 and 6 [34]. Except for vitexin, 4-O-feruloyliquinic acid, chlorogenic acid, scutellarin, apigenin, schaftoside, and genistein, the majority of substances have good polarity. Every compound exhibits a balanced level of saturation. Even if a chemical is biologically active, absorption may be hampered by a low logS value, whereas a high logS value suggests that a compound is readily digested and absorbed in the gastrointestinal system. The most soluble of all is 9-cis-retinal.

Molecular docking analysis

Molecular docking analysis of bioactive compounds against VEGFR2

The molecular docking results of bioactive compounds from *E. scaber* and Nintedanib are shown in **Table 3**. Nintedanib is a VEGFR inhibitor that plays an important role in non-small cell lung cancer (NSCLC) and idiopathic pulmonary fibrosis [35]. The interaction between Nintedanib and VEGFR forms five hydrogen bonds, three electrostatic bonds, and two hydrophobic interactions with the residues ASP1044, ARG1030, ARG1049, ASN1031, ASP1026, and ARG1025. The binding affinity of Nintedanib toward VEGFR is −7 kcal/mol. The visualization of the lowest binding affinity value is presented in **Figure 2**.

Table 3 Interaction between VEGFR and the bioactive compound from *E. scaber* extract.

Complexes	Binding energy (kcal/mol)	Interaction		
		Hydrogen bond	Hydrophobic	Electrostatic
Nintedanib (VEGFR inhibitor) – VEGFR	−7	**ARG1030, ARG1049 ASN1031**	-	**ASP1026, ASP1044**
Genistin – VEGFR	−10.1	GLU915, CYS917, GLU883, **ARG1049,** GLY920	LEU838, VAL846, VAL914, PHE916, ALA864, PHE1045, LEU1033, LYS866	-
Apigenin-7-O-glucuronide – VEGFR	−9.9	LEU838, GLU883, CYS917, ASN921, **ARG1049,** LEU838, PHE916	LEU838, LEU1033, PHE1045, ALA864, LEU1033, LEU838, VAL846, LYS866, VAL914	-
Luteolin – VEGFR	−9.6	**ASP1044,** CYS917, CYS917	LEU838, VAL914, LEU1033, PHE1045, LEU838, VAL846, ALA864, LYS866	-
Apigenin – VEGFR	−9.5	GLU883, CYS917, PHE916	LEU838, VAL914, LEU1033, LEU838, VAL846, ALA864, ALA864, LEU1033, VAL846, ALA864, LYS866	-
Pinocembrin – VEGFR	−9.5	CYS917, PHE916	LEU838, PHE1045, ALA864, LEU1033, VAL846, LYS866, VAL914	-
Scutellarin – VEGFR	−9.4	GLU883, CYS917, ASN921, **ARG1049,** PHE916	LEU838, LEU1033, PHE1045, ALA864, LEU1033, VAL846, LYS866, VAL914	-
Vitexin – VEGFR	−8.1	**ARG1025, ASP1044,** ALA879, ILE1042, ILE1023	HIS1024, LEU1017, ILE886	GLU883, **ASP1044**
(9cis)retinal – VEGFR	−7.5	**ARG1049**	LEU838, LEU1033, ALA864, LEU1033, VAL846, LYS866, VAL914, VAL897, CYS1043, PHE916, PHE1045, PHE1045	-
Feruloylquinic acid – VEGFR	−7.5	**ASP1044,** LEU838, CYS917, LEU838	PHE1045, LEU838, LYS866, VAL914, VAL846, VAL914	-

Complexes	Binding energy (kcal/mol)	Interaction		
		Hydrogen bond	Hydrophobic	Electrostatic
Shogaol – VEGFR	−7.2	**ASP1044**	VAL914, LEU838, LEU1033, LEU887, VAL897, CYS1043, LYS866, VAL897, PHE916, PHE1045	
4-methylumbelliferone – VEGFR	−7	**ASP1044,** PHE1045	VAL897, VAL914, LEU1033, CYS1043, VAL846, ALA864, LYS866, VAL914, CYS1043	
Caffeic acid – VEGFR	−6.8	GLU883	PHE1045, VAL846, CYS1043, VAL914	
3-methoxycinnamic acid – VEGFR	−6.3	**ASP1044,** PHE1045, CYS917	VAL846, PHE1045 CYS917, LEU1033, LEU838, ALA864, LEU1033, PHE916	

The amino acid residue of VEGFR bound by Nintedanib, ARG1049, is involved in several interactions, including VEGFR and Genistin via a conventional hydrogen bond; VEGFR and (9cis)retinal via two hydrogen bonds; VEGFR and Apigenin-7-O-glucuronide via a hydrogen bond; and VEGFR and Scutellarin via two hydrogen bonds. Meanwhile, another amino acid residue of VEGFR bound by Nintedanib, ARG1049, is involved in the interactions between VEGFR and 3-methoxycinnamic acid through a hydrogen bond; VEGFR and 4-methylumbelliferone through a hydrogen bond; VEGFR and Shogaol through a hydrogen bond; VEGFR and Luteolin through a hydrogen bond; VEGFR and Feruloylquinic acid through a hydrogen bond; and VEGFR and Vitexin through one hydrogen bond and two electrostatic interactions. In addition, the amino acid residue ARG1025, which Nintedanib also binds, forms a hydrogen bond with VEGFR and Vitexin. Among the compounds that can interact with the amino acid residues bound by Nintedanib, the three compounds with the most negative binding affinity values are Genistin (−10.1 kcal/mol), Apigenin-7-O-glucuronide (−9.9 kcal/mol), and Luteolin (−9.6 kcal/mol). All three have more negative binding affinities than Nintedanib (−7 kcal/mol) (**Table 3**).

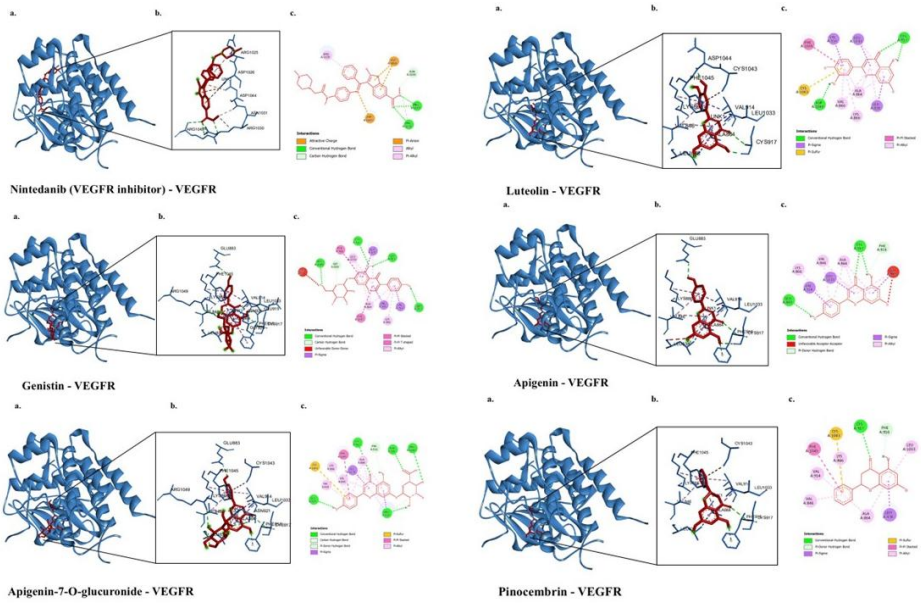

Figure 2 3D and 2D visualization of interactions between VEGFR and bioactive compounds in *E. scaber*. The representative visualization was obtained from the ligand that has the lowest binding affinity values compared to the inhibitor.

Molecular docking analysis of bioactive compounds against BCL2

The molecular docking results of bioactive compounds from *E. scaber* and Obatoclax are shown in **Figure 3**. Obatoclax is a BCL2 inhibitor [36]. The interaction between Obatoclax and BCL2 forms two hydrogen bonds with ASP103 and six hydrophobic interactions with the residues PHE104, ARG106, and ARG107 (**Table 4**). The binding affinity of Obatoclax toward BCL2 was −6.8 kcal/mol. The amino acid residue of BCL2 bound by Obatoclax, ARG106, is involved in the interaction between BCL2 and Genistin through a hydrophobic Pi-alkyl interaction, as well as in the interaction between BCL2 and Apigenin-7-O-glucuronide through two hydrogen bonds. Meanwhile, another amino acid residue bound by Obatoclax, PHE104, is involved in the interaction between 4-methylumbelliferone and BCL2 through three hydrophobic interactions, and in the interaction between BCL2 and Pinocembrin through one hydrogen bond. In addition, 4-methylumbelliferone can interact with other amino acid residues that are also bound by Obatoclax, such as ARG107 and ASP103, through four hydrogen bonds and one hydrophobic interaction, respectively. Among these compounds, only Apigenin-7-O-glucuronide has a more negative binding affinity than Obatoclax (−7.5 kcal/mol). Scutellarin has a more negative binding affinity than all other compounds (−7.8 kcal/mol); however, it does not bind to any amino acid residues that are shared with Obatoclax.

Table 4 Interaction between BCL2 and the bioactive compound from *E. scaber* extract.

Complexes	**Binding energy (kcal/mol)**	**Interaction**		
		Hydrogen bond	**Hydrophobic**	**Electrostatic**
Obatoclax - BCL-2	−6.8	**ASP103**	**PHE104, ARG106, ARG107**	
Genistin - BCL-2	−6.4	GLU152, SER105, GLU114, ARG109	**ARG106,** ARG109, ALA113	
3-methoxycinnamic acid - BCL-2	−5.8	ILE14, HIS94	TYR21, LYS17	

4-methylumbelliferone - BCL-2	−5.0	**ARG107, ASP103**	**PHE104,** TYR202, **ARG107**	
Caffeic acid - BCL-2	−5.7	HIS94, ILE14	TYR21, LYS17	
(9cis)retinal - BCL-2	−6.1	HIS94, ILE14	LYS17, ARG98, LEU95, TYR21, HIS94	
Shogaol - BCL-2	−5.5		TYR21, LYS17, ARG98, LEU97, TYR18, HIS94	
Pinocembrin - BCL-2	−5.9	**PHE104**	TYR202, ALA100	
Apigenin-7-O-glucuronide - BCL-2	−7.5	SER105, **ARG106,** SER116, GLN25	VAL159, ALA113, VAL156	LYS22
Scutellarin - BCL-2	−7.8	ARG109, ASP102, LYS22	VAL156, VAL159, ALA113	LYS22, ARG26
Apigenin - BCL-2	−6.1	ARG26, SER116	VAL156, ALA113	LYS22, GLU152
Luteolin - BCL-2	−6.4	ARG26, GLN25, ASP102	VAL156, ALA113	LYS22, GLU152
Feruloylquinic acid - BCL-2	−5.9	ARG26, SER116, GLU160, GLN25, ASP102	VAL156, ALA113	
Vitexin - BCL-2	−6.6	SER116, GLU160	VAL156, VAL159, ALA113	LYS22, GLU152

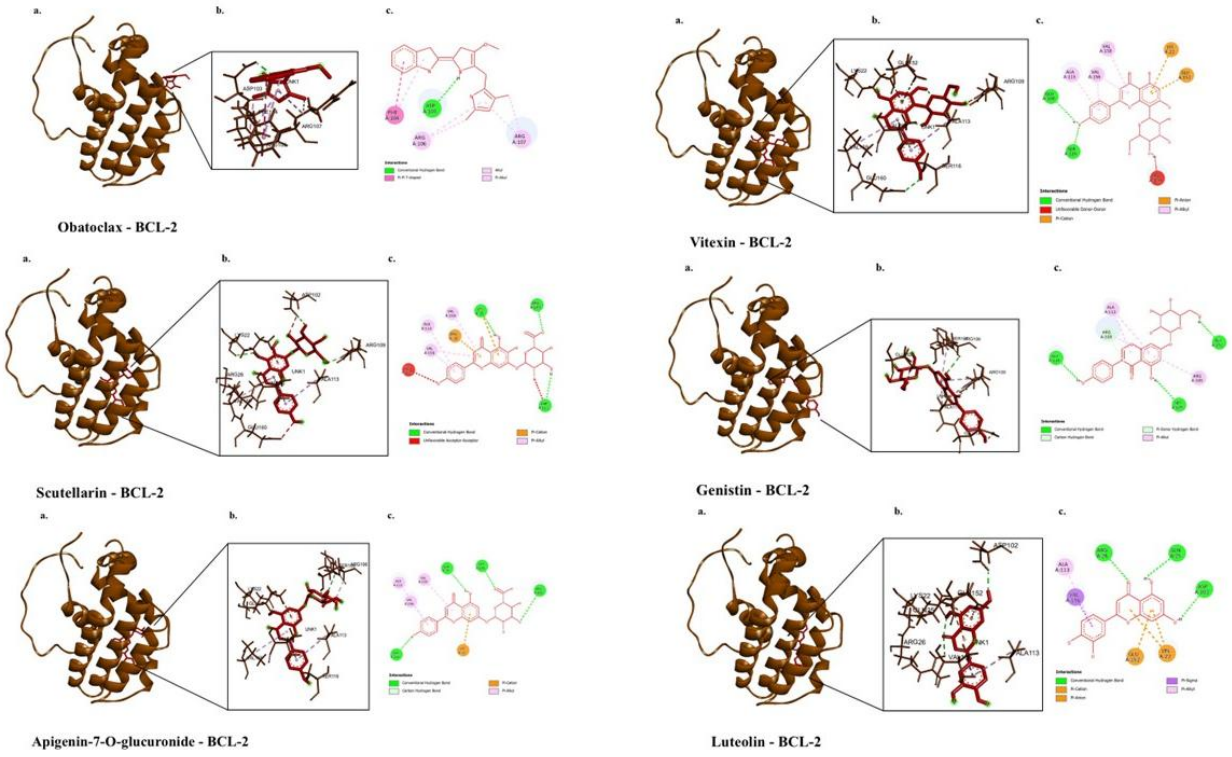

Figure 3 3D and 2D visualization of interactions between BCL2 and bioactive compounds in *E. scaber*. The representative visualization was obtained from the ligand that has the lowest binding affinity values compared to the inhibitor.

Molecular docking analysis of bioactive compounds against PI3K

The molecular docking results and visualization of bioactive compounds from *E. scaber* extract and Alpelisib are shown in **Table 5** and **Figure 4**. Alpelisib is a PI3K inhibitor used in cancer therapy [37]. The interaction between Alpelisib and PI3K forms nine hydrogen bonds with GLN859, VAL851, SER854, HIS855, and TYR836; eleven hydrophobic interactions with VAL851, MET922, ILE932, MET772, ILE800, ILE848, TRP780, TYR836, HIS855, PHE930, and VAL850; and one additional type of interaction, a Pi-sulfur bond with MET922. The binding affinity of Alpelisib toward PI3K is −10.5 kcal/mol. All investigated compounds from *E. scaber* can interact with the amino acid residues involved in Alpelisib binding to PI3K, such as GLN859, VAL851, SER854, HIS855, TYR836, MET922, ILE932, ILE800, ILE848, TRP780, TYR836, and VAL850. All the compounds exhibit more positive binding affinity values than Alpelisib. Among these compounds, the three with the most negative binding affinities are Apigenin-7-O-glucuronide (−9.7 kcal/mol), Genistin (−9.3 kcal/mol), and Scutellarin (−9.2 kcal/mol), respectively.

Table 5 Interaction between PI3K and the bioactive compound from *E. scaber* extract.

Complexes	Binding energy (kcal/mol)	Interaction	
		Hydrogen bond	Hydrophobic
Alpelisib – PI3K	−10.5	GLN859, VAL851, SER854, SER854, GLN859, VAL851, HIS855, VAL851, TYR836	VAL851, MET922, ILE932, MET772, ILE800, ILE848, TRP780, TYR836, HIS855, PHE930, VAL850
Apigenin-7-O-glucuronide – PI3K	−9.7	LYS802, **TYR836,** CYS838, **VAL851,** ASP933, **TYR836**	**TRP780, TYR836, ILE932, VAL850**
Genistin – PI3K	−9.3	TYR836, SER854, HIS855	MET922, ILE932, TRP780, TYR836, VAL850, ILE848
Scutellarin – PI3K	−9.2	ARG770, **GLN859,** GLU768, **VAL851**	**MET922, TRP780, HIS855, VAL850, VAL851, MET922**
Vitexin – PI3K	−8.7	SER774, SER919, ASP933	**TYR836, ILE932, ILE848, ILE932, ILE848, ILE932**
Luteolin – PI3K	−8.5	**VAL851**	**ILE932, TYR836, ILE848, ILE848, ILE932, ILE932**
Apigenin – PI3K	−8.4	CYS838, **SER854, VAL851**	**ILE848, TYR836, ILE848, ILE932**
Pinocembrin – PI3K	−8.2	LYS802, ASP933	**ILE848, ILE932, TYR836, VAL851, MET922**
Feruloylquinic acid – PI3K	−7.6	LYS802, **VAL851, SER854,** ASP933	**TRP780, ILE848, ILE932**
(9cis)retinal – PI3K	−7.4	-	**TYR836, ILE932, VAL851, ILE932, ILE800, ILE848, MET922, VAL850, MET922, TRP780, TYR836**
Shogaol – PI3K	−6.7	**TYR836, VAL851**	**VAL850, MET922,** CYS838, **ILE848, TRP780, TYR836, ILE848, ILE932**
4-methylumbelliferone – PI3K	−6.6	TYR836, VAL851, ASP933, GLU849	ILE932, TYR836, ILE848, ILE932

Complexes	Binding energy (kcal/mol)	Interaction	
		Hydrogen bond	Hydrophobic
Caffeic acid – PI3K	−6.6	**TYR836,** GLU849	**TYR836, ILE848, ILE932**
3-methoxycinnamic acid – PI3K	−6.2	TYR836	ILE932, TYR836, VAL850, MET922, VAL851, MET922, TRP780

The molecular docking results revealed that several bioactive compounds from *E. scaber* inhibited proteins such as VEGFR2, BCL2, and PI3K. VEGFR2, a subtype of VEGFR, is a tyrosine kinase receptor that binds VEGF and contributes to the mechanisms of metastasis, tumor cell invasion, and tumor angiogenesis in various types of cancer [38]. Therefore, VEGFR2 represents a promising target in cancer therapy. The docking results for VEGFR revealed several compounds that occupy the same binding site as Nintedanib, used as a positive control, as evidenced by the similarity of the amino acid residues bound by these compounds to those bound by Nintedanib. Among these compounds, Genistin, Apigenin-7-O-glucuronide, and Luteolin exhibited the strongest binding affinities among the other compounds and Nintedanib, as indicated by their lower (more negative) binding affinity scores [39]. Among the three, Genistin binds VEGFR with the strongest affinity, forming five hydrogen bonds with GLU915, GLU883, CYS917, ARG1049, and GLY920; thirteen hydrophobic interactions with LEU838, VAL846, VAL914, PHE916, PHE1045, ALA864, LEU1033, LEU838, ALA864, LEU1033, and LYS866; and one unfavorable bond with ASN921. Previous studies have reported that Genistin can influence VEGFR through direct suppression or inhibition of the estrogen receptor pathway that enhances its expression [40]. Meanwhile, BCL2 is an anti-apoptotic protein capable of binding pro-apoptotic proteins such as Bax and Bak, as well as BH3-only proteins, thereby playing a crucial role in the inhibition of intrinsic apoptosis. BCL2 has often been reported to contribute to various cancers and drug resistance, making it an attractive target in cancer therapy [41].

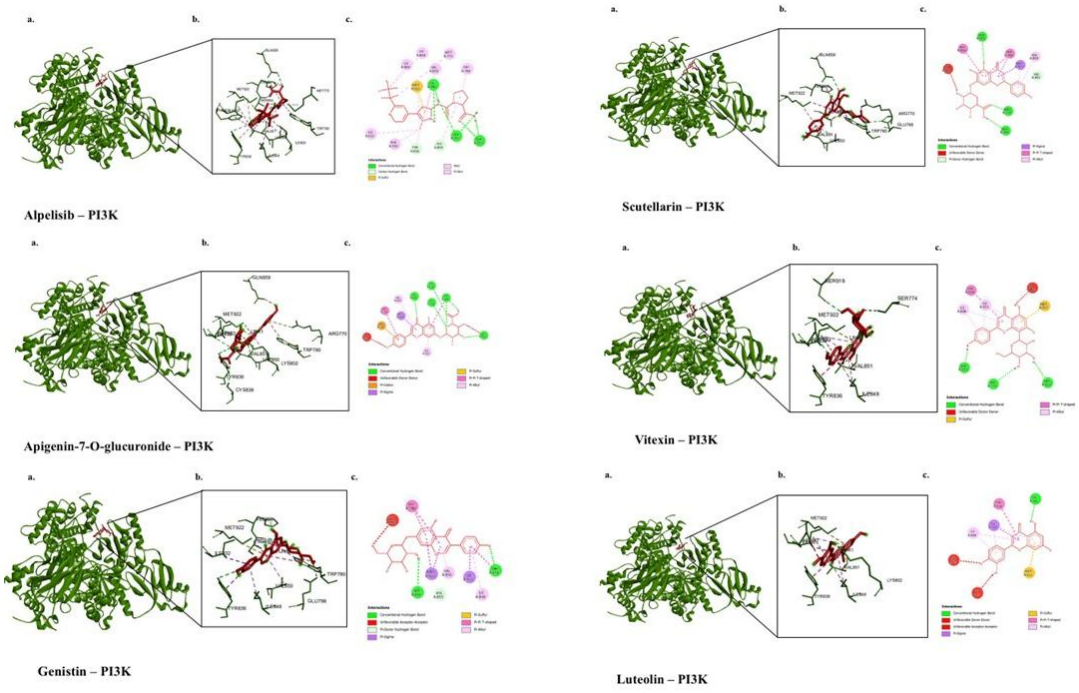

Figure 4 3D and 2D visualization of interactions between PI3K and bioactive compounds in *E. scaber*. The representative visualization was obtained from the ligand that has the lowest binding affinity values compared to the inhibitor.

The docking results for BCL2 revealed several compounds that occupy the same binding site as Obatoclax, used as a positive control, as evidenced by the similarity of the amino acid residues bound by these compounds to those bound by Obatoclax. Only Apigenin-7-O-glucuronide showed a higher binding affinity than Obatoclax among these substances, as seen by its lower (more negative) binding affinity score. BCL2 is bound by apigenin-7-O-glucuronide via three hydrophobic contacts with VAL159, ALA113, and VAL156; five hydrogen bonds with SER105, ARG106, SER116, GLN25, and ARG106; and an electrostatic bond with LYS22. According to earlier research, Apigenin-7-O-glucuronide can promote cellular death by inducing cytochrome c release through the modulation of Bcl-2 family proteins [42]. Conversely, PI3K is an important enzyme in signaling pathways that control cell survival, growth, metabolism, and proliferation [43]. PI3K is a therapeutic target in several cancer types because mutations and overactivation of PI3K contribute to different types of cancer. As demonstrated by the similarity of the amino acid residues bound by these compounds to those bound by Alpelisib, the docking data for PI3K showed that all of the *E. scaber* compounds examined in this investigation occupied the same binding site as Alpelisib, which was utilized as a positive control. Compared to alpelisib, all of these substances had lower binding affinities for PI3K. The three chemicals with the highest binding affinities are Scutellarin, Genistin, and Apigenin-7-O-glucuronide, in descending order. Apigenin-7-O-glucuronide binds PI3K by forming six hydrogen bonds with LYS802, TYR836, CYS838, VAL851, ASP933, and TYR836; one electrostatic bond with ARG770; five hydrophobic interactions with MET922, TRP780, TYR836, ILE932, and VAL850; two unfavorable bonds with LYS802 and GLN859; and one Pi-sulfur interaction with MET922According to earlier research, Apigenin-7-O-glucuronide can alter PI3K-related signaling pathways in lung and cervical cancer [42,44].

Molecular dynamics simulation

The best-scoring docking poses (lowest binding energy) for each protein–ligand complex were further evaluated by 20 ns molecular dynamics (MD) simulations. Complex stability was assessed using the root-mean-square deviation (RMSD) of the protein backbone and the root-mean-square fluctuation (RMSF) of individual residues. RMSD reflects the overall structural deviation of the protein during the simulation; backbone RMSD values fluctuating around or below ~3 Å are generally considered indicative of a stable conformation [45]. RMSF, in turn, describes the flexibility of each amino acid residue, where the majority of residues showing fluctuations below 3 Å suggests that the global protein fold remains stable [46].

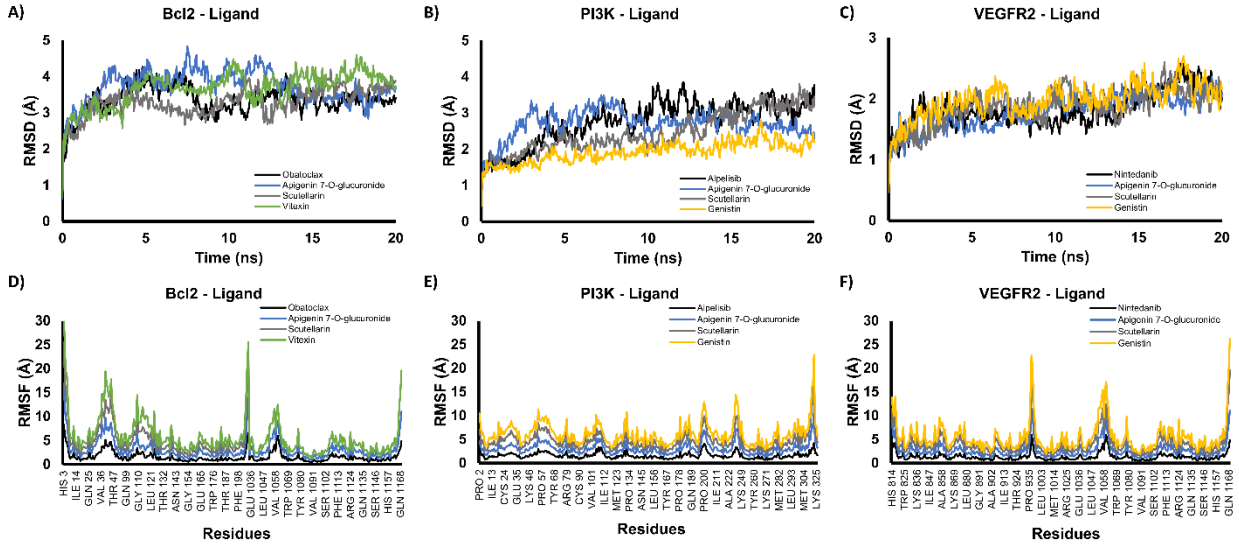

Figure 5 Molecular dynamics simulations of protein–ligand complexes. Backbone RMSD profiles for BCL2–ligand (A), PI3K–ligand (B), and VEGFR2–ligand (C) complexes, and RMSF profiles for BCL2–ligand (D), PI3K–ligand (E), and VEGFR2–ligand (F) complexes.

For BCL2, both the RMSD and RMSF profiles of the complex with the active compound closely resembled those of the control (Obatoclax), with no large deviations observed throughout the simulation (**Figures 5(A)** and **5(D)**). Similarly, the PI3K complexes displayed comparable RMSD and RMSF patterns between the active compound and the control, and their trajectories remained stable over the 20 ns run (**Figures 5(B)** and **5(E)**). The VEGFR2–ligand complex showed the most stable backbone dynamics, with RMSD values consistently below 3 Å (**Figure 5(C)**), and its RMSF profile did not differ markedly from that of the control (**Figure 5(F)**). The MD simulations indicate that binding of the active compounds to BCL2, PI3K, and VEGFR2 does not destabilize the protein structures and that all three complexes remained structurally stable during the 20 ns simulations, supporting the reliability of the docking poses and the feasibility of these interactions under dynamic conditions. These findings were only from computational models, which demonstrated that bioactive compounds from *E. scaber* possessed multitarget inhibitor potential via inhibition of VEGFR2, BCL2, and PI3K. Therefore, further experimental validation, including *in vitro* and *in vivo* studies to confirm their anticancer activity, is needed.

Conclusions

This study demonstrates that several bioactive compounds from *E. scaber* exhibit strong multi-target inhibitory potential against key cancer-related proteins, including VEGFR2, BCL2, and PI3K. Notably, apigenin-7-O-glucuronide and genistin demonstrated favorable interactions and consistently high binding affinities better than those of reference inhibitors. These *in silico* findings support *E. scaber* as a promising source of anticancer phytochemicals and provide a molecular basis for further *in vitro* and *in vivo* validation.

Acknowledgements

The author thanks the Directorate General of Research and Development Program, Ministry of Higher Education, Science, and Technology, for funding this research through the Fundamental Research with grant no. 064/C3/DT.05.00/PL/2025 and 630/UN10.A0501/B/PT.01.03.2/2025.

Declaration of Generative AI in Scientific Writing

This manuscript preparation did not use any generative AI tools. No content or data interpretation was executed by generative AI. All authors are responsible for the content and conclusion of this work

CRediT Author Statement

Yuyun Ika Christina: Conceptualization; Methodology, Investigation, Data Curation, Project administration, Writing - Original Draft, Writing - Review & Editing. **Shella Zahra Kumala Azmi:** Formal analysis; Writing - Original Draft. **Wirdatun Nafisah:** Visualization; Formal analysis. **Honesty Nurizza Pinanty:** Visualization; Investigation, Formal analysis, Writing - Original Draft. **Muhammad Hermawan Widyananda:** Software; Validation. **Sutrisno Sutrisno:** Writing - Reviewing and Editing. **Elok Zubaidah:** Writing - Review & Editing. **Husnul Khotimah:** Writing - Review & Editing. **Muhammad Sasmito Djati:** Conceptualization, Funding acquisition, Supervision, Writing - Review & Editing.

References

[1] MK Hong and DC Ding. Early diagnosis of ovarian cancer: A comprehensive review of the advances, challenges, and future directions. *Diagnostics* 2025; **15(4)**, 406.

[2] VM Ettorre, A AlAshqar, N Sethi and AD Santin. Personalized treatment in ovarian cancer: A review of disease monitoring, biomarker expression, and targeted treatments for advanced, recurrent ovarian cancers. *Cancers* 2025; **17(11)**, 1822.

[3] World Ovarian Cancer Coalition. Ovarian Cancer Data Briefing 2024. Available at: https://worldovariancancercoalition.org/wp-content/uploads/2024/04/2024-Global-Priority.pdf, accessed December 2025.

[4] Globocan. Estimated number of new cases from 2022 to 2050, Incidence, Both sexes, age [0-85+]. Globocan 2022 (version 1.1) - 08.02.2024. International Agency for Research on Cancer (IARC) 2022. Available at: https://gco.iarc.fr/tomorrow/en/dataviz/tables?cancers=25&single_unit=10000&years=2050, accessed December 2025.

[5] The International Association for Cryptologic Research. Data visualization tools for exploring the global cancer burden in 2022. Available at: https://gco.iarc.who.int/today, accessed December 2025.

[6] S Linus-Lojikip, V Subramaniam, L Wei-Yin Lim and H Amar-Singh. Survival of patients with advanced and recurrent ovarian cancer treated using integrative medicine in Malaysia: A case series. *Complementary Therapies in Clinical Practice* 2019; **37**, 73.

[7] C Lliberos, G Richardson and A Papa. Oncogenic pathways and targeted therapies in ovarian cancer. *Biomolecules* 2024; **14(5)**, 585.

[8] YI Christina, M Rifa'i, N Widodo and MS Djati The combination of *Elephantopus scaber* and *Phaleria macrocarpa* leaf extracts promotes anticancer activity via downregulation of ER-α, Nrf2, and the PI3K/AKT/mTOR pathway. *Journal of Ayurveda and Integrative Medicine* 2022; **13(4)**, 100674.

[9] MDT Hossain and MdA Hossain. Targeting PI3K in cancer treatment: A comprehensive review with insights from clinical outcomes. *European Journal of Pharmacology* 2025; **996**, 177432.

[10] TT Huang, EJ Lampert, C Coots and JM Lee. Targeting the PI3K pathway and DNA damage response as a therapeutic strategy in ovarian cancer. *Cancer Treatment Reviews* 2020; **86**, 102021.

[11] M Vogler, Y Braun, VM Smith, MA Westhoff, RS Pereira, NM Pieper, M Anders, M Callens, T Vervliet, M Abbas, S Macip, R Schmid, G Bultynck and MJ Dyer. The BCL2 family: From apoptosis mechanisms to new advances in targeted therapy. *Signal Transduction and Targeted Therapy* 2025; **10**, 91

[12] FH Shah, YS Nam, JY Bang, IS Hwang, DH Kim, M Ki and HW Lee. Targeting vascular endothelial growth receptor-2 (VEGFR-2): Structural biology, functional insights, and therapeutic resistance. *Archives of Pharmacal Research* 2025; **48(5)**, 404.

[13] MS Djati and YI Christina. Traditional Indonesian rempah-rempah as a modern functional food and herbal medicine. *Functional Foods in Health and Disease* 2019; **9(4)**, 241-264.

[14] MS Djati, YI Christina and M Rifa'i. The combination of *Elephantopus scaber* and *Sauropus androgynus* promotes erythroid lineages and modulates follicle-stimulating hormone and luteinizing hormone levels in pregnant mice infected with *Escherichia coli*. *Veterinary World* 2021; **14(5)**, 1398-1404.

[15] FA Kabeer, DS Rajalekshmi, MS Nair, R Prathapan. *In vitro* and *in vivo* antitumor activity of deoxyelephantopin from a potential medicinal plant *Elephantopus scaber* against Ehrlich ascites carcinoma. *Biocatalysis and Agricultural Biotechnology* 2019; **19**, 101106.

[16] CK Chan, G Chan, K Awang and HA Kadir. Deoxyelephantopin from *Elephantopus scaber* inhibits HCT116 human colorectal carcinoma cell growth through apoptosis and cell cycle arrest. *Molecules* 2016; **21(3)**, 385.

[17] YI Christina, W Nafisah, MF Atho'Illah, M Rifa'i, N Widodo and MS Djati. Anti-breast cancer potential activity of Phaleria macrocarpa (Scheff.) Boerl. leaf extract through *in silico* studies. *Journal of Pharmacy & Pharmacognosy Research* 2021; **9(6)**, 824-845.

[18] AE Alghoull, SR Firdausi, YI Christina, S Widyarti, M Rifa'i and MS Djati. Evaluating the efficacy of ethanolic extract of Tapak Liman (*Elephantopus scaber* L.) leaf in inhibiting pulmonary fibrosis: Mechanisms through anti-fibrotic cytokine promotion. *Open Veterinary Journal* 2025; **15(1)**, 118-125.

[19] S Pellacani, C Citti, L Strani, B Benedetti, PP Becchi, V Pizzamiglio, S Michelini, G Cannazza, ADE Juan, M Cocchi and C Durante. Comparative analysis of features extraction protocols for LC-HRMS untargeted metabolomics in mountain cheese 'identitation'. *Microchemical Journal* 2024; **207**, 111863.

[20] W Nafisah, F Fatchiyah, MH Widyananda, YI Christina, M Rifa'i, N Widodo and MS Djati. Potential of bioactive compound of *Cyperus rotundus* L. rhizome extract as inhibitor of PD-L1/PD-1 interaction: An *in silico* study. *Agriculture and Natural Resources* 2022; **56(4)**, 751-760.

[21] MH Widyananda, ST Wicaksono, K Rahmawati, S Puspitarini, SM Ulfa, YD Jatmiko, M Masruri and N Widodo. A potential anticancer mechanism of finger root (*Boesenbergia rotunda*) extracts against a breast cancer cell line. *Scientifica* 2022; **2022**, 9130252.

[22] LK Muharrami, M Santoso and S Fatmawati. Chemical profiles, *in silico* pharmacokinetic and toxicity prediction of bioactive compounds from *Boesenbergia rotunda*. *Case Studies in Chemical and Environmental Engineering* 2024; **10**, 100992.

[23] A Shofiah, YI Christina, DR Dwijayanti, A Soewondo, N Widodo and MS Djati. Exploring the inflammatory pathway modulation of *Phaleria macrocarpa*: Evidence from *in vitro* and *in silico* studies. *Pharmacia* 2025; **72**, 1-14.

[24] SH Abdullahi, AT Moin, A Uzairu, AB Umar, MT Ibrahim, MT Usman, N Nawal, I Bayil and T Zubair. Molecular docking studies of some benzoxazole and benzothiazole derivatives as VEGFR-2 target inhibitors: *In silico* design, MD simulation, pharmacokinetics and DFT studies. *Intelligent Pharmacy* 2024; **2(2)**, 232-250.

[25] C Kirubhanand, J Selvaraj, UV Rekha, V Vishnupriya, V Sivabalan, M Manikannan, D Nalini, P Vijayalakshmi, M Rajalakshmi and R Ponnulakshmi. Molecular docking analysis of Bcl-2 with phyto-compounds. *Bioinformation* 2020; **16(6)**, 468-473.

[26] X Liu, S Yang, JR Hart, Y Xu, X Zou, H Zhang, Q Zhou, T Xia, Y Zhang, D Yang, M Wang and PK Vogt. Cryo-EM structures of PI3Kα reveal conformational changes during inhibition and activation. *Proceedings of the National Academy of Sciences* 2021; **118(45)**, e2109327118,

[27] MH Widyananda, N Rosyada, L Muflikhah, N Widodo, DR Dwijayanti and SM Ulfa. Lagerstroemin from *Lagerstroemia speciosa* as antibreast cancer candidate targeting AURKA, EGFR and SRC Protein: A comprehensive computational study. *Trends in Sciences* 2024; **21(10)**, 8205.

[28] MH Widyananda, F Fatchiyah, L Muflikhah, SM Ulfa and N Widodo. Computational examination to reveal Kaempferol as the most potent active compound from Euphorbia hirta against breast cancer by targeting AKT1 and ERα. *Egyptian Journal of Basic and Applied Sciences* 2023; **10(1)**, 753-767.

[29] HS Tuli, P Rath, A Chauhan, K Sak, D Aggarwal, R Choudhary, U Sharma, K Vashishth, S Sharma, M Kumar, V Yadav, T Singh, MB Yerer and S Haque. Luteolin, a potent anticancer compound: From chemistry to cellular interactions and

synergetic perspectives. *Cancers* 2022; **14(21)**, 5373.

[30] K Mogi, Y Koya, M Yoshihara, M Sugiyama, R Miki, E Miyamoto, H Fujimoto, K Kitami, S Iyoshi, S Tano, K Uno, S Tamauchi, A Yokoi, Y Shimizu, Y Ikeda, N Yoshikawa, K Niimi, Y Yamakita, H Tomita, K Shibata, A Nawa, Y Tomoda and H Kajiyama. 9-oxo-ODAs suppresses the proliferation of human cervical cancer cells through the inhibition of CDKs and HPV oncoproteins. *Scientific Reports* 2023; **13(1)**, 19208.

[31] M Redka, S Baumgart, D Kupczyk, T Kosmalski and R Studzińska. Lipophilic studies and in silico ADME profiling of biologically active 2-Aminothiazol-4(5H)-one derivatives. *International Journal of Molecular Sciences* 2023; **24(15)**, 12230.

[32] S Chander, CR Tang, HM Al-Maqtari, J Jamalis, A Penta, TB Hadda, HM Sirat, YT Zheng and M Sankaranarayanan. Synthesis and study of anti-HIV-1 RT activity of 5-benzoyl-4-methyl-1,3,4,5-tetrahydro-2H-1,5-benzodiazepin-2-one derivatives. *Bioorganic Chemistry* 2017; **72**, 74-79.

[33] LZ Benet, CM Hosey, O Ursu and TI Oprea. BDDCS, the Rule of 5 and drugability. *Advanced Drug Delivery Reviews* 2016; **101**, 89-98.

[34] ANS Kamble and AA Mitkar. Swiss ADME predictions of pharmacokinetics and drug-likeness properties of secondary metabolites present in *Trigonella foenum-graecum*. *Journal of Pharmacognosy and Phytochemistry* 2023; **12(5)**, 341-349.

[35] S Yan, S Xue, T Wang, R Gao, H Zeng, Q Wang and X Jia. Efficacy and safety of nintedanib in patients with non-small cell lung cancer, and novel insights in radiation-induced lung toxicity. *Frontiers in Oncology* 2023; **13**, 1086214.

[36] J Li, J Xu and Z Li. Obatoclax, the pan-Bcl-2 inhibitor sensitizes hepatocellular carcinoma cells to promote the anti-tumor efficacy in combination with immune checkpoint blockade. *Translational Oncology* 2021; **14**, 101116.

[37] F André, E Ciruelos, G Rubovszky, M Campone, S Loibl, HS Rugo, H Iwata, P Conte, IA Mayer, B Kaufman, T Yamashita, L Yen-Shen, K Inoue, M Takahashi, Z Pápai, L Anne-Sophie, D Mills, C Wilke, S Hirawat, D Juric and SOLAR-1 Study Group. Alpelisib for *PIK3CA*-Mutated, hormone receptor-positive advanced breast cancer. *The New England Journal of Medicine* 2019; **380(20)**, 1929-1940.

[38] J Zeng, Q Deng, Z Chen, S Yan, Q Dong, Y Zhang, Y Cui, L Li, Y He and J Shi. Recent development of VEGFR small molecule inhibitors as anticancer agents: A patent review (2021 - 2023). *Bioorganic Chemistry* 2024; **146**, 107278.

[39] Z Amiri, M Bayat and D Gheidari. Synthesis of thiazoloquinolinone derivatives: Molecular docking, MD simulation, and pharmacological evaluation as VEGFR-2 inhibitors. *BMC Chemistry* 2025; **19**, 90.

[40] Z Javed, K Khan, J Herrera-Bravo, S Naeem, MJ Iqbal, H Sadia, QR Qadri, S Raza, A Irshad, A Akbar, Ž Reiner, A Al-Harrasi, A Al-Rawahi, D Satmbekova, M Butnariu, IC Bagiu, RV Bagiu and J Sharifi-Rad. Genistein as a regulator of signaling pathways and microRNAs in different types of cancers. *Cancer Cell International* 2021; **21**, 388.

[41] S D'Aguanno and DD Bufalo. Inhibition of anti-apoptotic Bcl-2 proteins in preclinical and clinical studies: Current overview in cancer. *Cells* 2020; **9(5)**, 1287.

[42] MM Liu, RH Ma, ZJ Ni, K Thakur, CL Cespedes-Acuña, L Jiang and ZJ Wei. Apigenin 7-O-glucoside promotes cell apoptosis through the PTEN/PI3K/AKT pathway and inhibits cell migration in cervical cancer HeLa cells. *Food and Chemical Toxicology* 2020; **146**, 111843.

[43] IM Bastos, S Rebelo and VLM Silva. A comprehensive review on phosphatidylinositol-3-kinase (PI3K) and its inhibitors bearing pyrazole or indazole core for cancer therapy. *Chemico-Biological Interactions* 2024; **398**, 111073.

[44] C Chen, S Zhong, H Wu, J Ge and Q Wang. Apigenin-7-glucoside induces apoptosis and ROS accumulation in lung cancer cells, and inhibits PI3K/Akt/mTOR pathway. *Tropical Journal of Pharmaceutical Research* 2023; **22(5)**, 937-943.

[45] N Kumar, D Sood, R Tomar and R Chandra. Antimicrobial peptide designing and optimization employing large-scale flexibility analysis of

protein-peptide fragments. *ACS Omega* 2019; **4(25)**, 21370-21380.

[46] TL Wargasetia, H Ratnawati, N Widodo and MH Widyananda. Bioinformatics study of sea cucumber peptides as antibreast cancer through inhibiting the activity of overexpressed protein (EGFR, PI3K, AKT1, and CDK4). *Cancer Informatics* 2021; **20**, 117693512110318.